IEEE Access
Multidisciplinary ⋮ Rapid Review ⋮ Open Access Journal

Received 10 May 2022, accepted 23 May 2022, date of publication 22 June 2022, date of current version 29 June 2022.

Digital Object Identifier 10.1109/ACCESS.2022.3185188

Deep Learning Modeling of a WBAN-MIMO Channel in Underground Mine

KHALED KEDJAR[1,2], (Member, IEEE), MOULAY ELHASSAN ELAZHARI[2,3], (Member, IEEE), LARBI TALBI[1], (Senior Member, IEEE), AND MOURAD NEDIL[2], (Senior Member, IEEE)

[1]Computer Sciences and Engineering Department, University of Quebec in Outaouais, Gatineau, QC J8X 3X7, Canada
[2]School of Engineering, Université du Québec en Abitibi-Témiscamingue (UQAT), Val-d'Or, QC J9P 1Y3, Canada
[3]School of Science and Engineering, Al Akhawayn University, Ifran 53003, Morocco

Corresponding author: Khaled Kedjar (kedk01@uqo.ca)

The work was supposed by the Fond de Recherche du Québec-Nature et Technologie (FRQNT).

ABSTRACT In this study, an efficient model of the channel matrix is developed for a 2 × 2 wireless body area network multiple input output (WBAN-MIMO) system based on deep learning algorithms. The model is composed of three deep-learning algorithms. Moreover, the model simultaneously predicts channel matrix H in an underground mine and identifies the position of the collected data in both line-of-sight (LoS) and non-line-of-sight (NLoS) scenarios. The model was trained and evaluated using the magnitude and phase of the collected data in an underground mine environment within a frequency range of 2.3 GHz – 2.5 GHz. These measurements, conducted with different antenna configurations in the LoS and NLoS scenarios, constitute an input to the model. The latest predicts the channel matrix $\boldsymbol{H}$ with position and identifies whether the channel is a LoS or NLoS. Finally, the path loss and channel impulse response models were compared with measurement-based models. The modeled channel prediction exhibited a lower root mean square error (RMSE) for channel prediction and high classification accuracy for LoS-NLoS and position identification, respectively. The numerical results reveal that deep learning WBAN-MIMO modeling offers a powerful solution for future wireless systems in underground mine environments.

INDEX TERMS Channel models, capacity, deep learning, impulse response, multipath channel, MIMO channel, LSTM, path loss, WBAN.

I. INTRODUCTION

Multiple-input multiple-output (MIMO) technology provides numerous advantages over a single-input single-output (SISO) system. These advantages have helped increase the Internet of Things (IoT) technologies owing to the increased bit rate for MIMO [1]. The main known advantages of IoT are the monitoring of data, control, automation, and safety in many areas, whether in military or civil areas [2], [3]. In this work, the focus is on civil areas, explicitly in underground mine environments. Therefore, to improve the miners' safety and wireless communications systems, several studies demonstrated a great interest in Wireless Body Area network (WBAN) using MIMO systems [1], [4]–[6]. It was shown that owing to the variation in the human body geometry, different trajectories of signals with similar lengths significantly affect the propagation mechanism [4]. Moreover, theoretical and experimental studies have confirmed that MIMO technology offers better efficiency for wireless systems and increases the channel capacity of WBAN [4], [7]–[10]. Even though studies have published good channel modeling and characterization results, they remain insufficient in terms of accuracy. In fact. statistical and empirical models [8], [11]–[14] are cite-specific and have not been proven for general underground applications. Through the process of model validation, extensive data were collected from the experimental measurements. The experimental procedures had undergone Line of the Sight (LoS) or non-LoS (NLoS) scenarios, using different antenna combinations and configurations. Hence, one can conclude that the Deep Learning (DL) algorithms, adapted to learn the patterns within big data collections [15] can be used to model the channel propagation within any antenna combination and configuration. DL algorithms have been applied in the past few years to outdate traditional models and provide new solutions to localization [16] and channel prediction accuracy [17]. *Luo et al.* [17]

The associate editor coordinating the review of this manuscript and approving it for publication was Fang Yang.

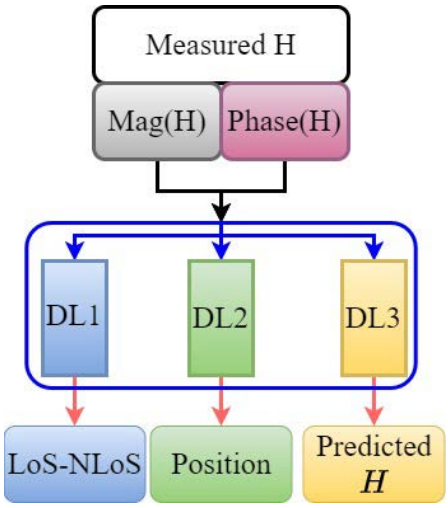

FIGURE 1. The framework diagram to illustrate the main input and outputs of the proposed stacked model.

introduced a DL model based on Long Short Term with Memory (LSTM) networks to predict a Single Input Single output (SISO) channel. *Ding et al.* [18] used a complex-valued neural network to forecast frequency-domain channel characteristics. *Jiang et al.* [19] provided a novel MIMO channel predictor built on a deep recurrent neural network (RNN) that incorporates LSTMs or gated recurrent unit (GRUs) memory cells. Convolutional neural networks combined with recurrent neural network design (CNN-RNN) to predict CSI have been proposed in [20]–[22]. *Arnold et al.* [23] investigated the feasibility of DL algorithms for MIMO configurations based on orthogonal Frequency Division Multiplex (OFDM). Dense layers were used with two-step training strategies to predict the NLOS position. However, these techniques are considered efficient tools for applying the DL algorithm to CSI prediction and LOS-NLOS detection. This requires high computational complexity, especially in harsh environments, and data processing is still ambiguous, which is crucial for DL algorithms. Therefore, a new efficient technique is needed, especially for the WBAN– MIMO channel, which is essential for improving miners' safety. The DL model can help new cloud IoT technologies provide a solution to miners' safety and machinery control. The solution model must provide crucial information, such as whether the channel is in the LoS or NLoS, where the receiver is located away from the transmitter and channel prediction. In this study, a novel scheme was proposed to predict the WBAN-MIMO channel in underground mine environments considering different antenna polarizations.

To the best of the authors' knowledge, no modeling technique has been developed to model the WBAN-MIMO channel in an underground mine environment. The novelty of this study can be summarized as follows.

- First, a stacked model (SM) is proposed to predict the MIMO channel matrix H for LoS and NLoS scenarios.
- Second, the SM modeling framework was designed based on three parallel DL-LSTM networks. The framework was introduced to simultaneously estimate classification and regression, as illustrated in Figure 1.
- The SM model simultaneously predicts the channel matrices of Mag(H) and Phase(H), classifies the position of the collected data, and identifies whether these data are in LoS or NLoS scenarios.

Several measurement campaigns were conducted to support the proposed modelling technique. These data were also explored in [4] (by our group), where they proposed a new solution for future Body to Body (B2B) applications using both circularly and linearly polarized antennas. In terms of path loss (PL), RMS delay spread, and channel capacity, the circularly polarized setup outperformed the other topologies. Owing to the large increase in PL, the NLOS scenario resulted in a severe reduction in the channel capacity.

II. STACKED MODEL PREDICTION SCHEME

As mentioned previously, DL modelling is based on a large number of experimental measurements. Therefore, designing a scheme for channel prediction is crucial. Hence, several stacked modelling techniques have been suggested in the literature for univariate and multivariate forecasting. *Seongchan Kim et al.* [24] used the ConvLSTM stacked model to forecast rainfall using radar channel data. This technique was more effective than the use of fully connected LSTM networks. *An et al.* [25] introduced a hybrid model that combines a CNN with a stacked LSTM network. *Le Sun et al.* [26] used a stacked LSTM network to detect the atrial using electrocardiography (ECG) data. This technique achieved high prediction accuracy using stacked modeling. Additionally, regarding stock market forecasting, *Althelaya et al.* [27] proposed a stacked model based on LSTM and GRU. As a result, the stacked LSTM model achieved a higher performance than the baseline and GRU-based models. In this paper, a stacked modeling technique for a WBAN-MIMO prediction scheme was presented and compared to the model published in [28]. The model (which is based on LSTM network) is used to predict the SISO channel in different environments with low prediction errors of less than 2% Mean Square Error (MSE). First, a channel prediction framework was introduced and expressed as a regression problem [29]. Then, the position and LoS-NLoS classification [29] schemes are presented. As illustrated in Figure 2, the proposed prediction scheme was constructed using different modules. First, the data-processing module was used to prepare the data for the training and validation processes. The SM model simultaneously predicts each sub-channel of the matrix $\boldsymbol{H}$ at each measured position using the magnitude (Mag($\boldsymbol{H}$)) and phase (Phase($\boldsymbol{H}$)) of the same input as the channel prediction scheme, position, and LoS-NLoS classifiers. Therefore, categorical and binary classifications were considered for the position and LoS-NLoS scenarios, respectively.

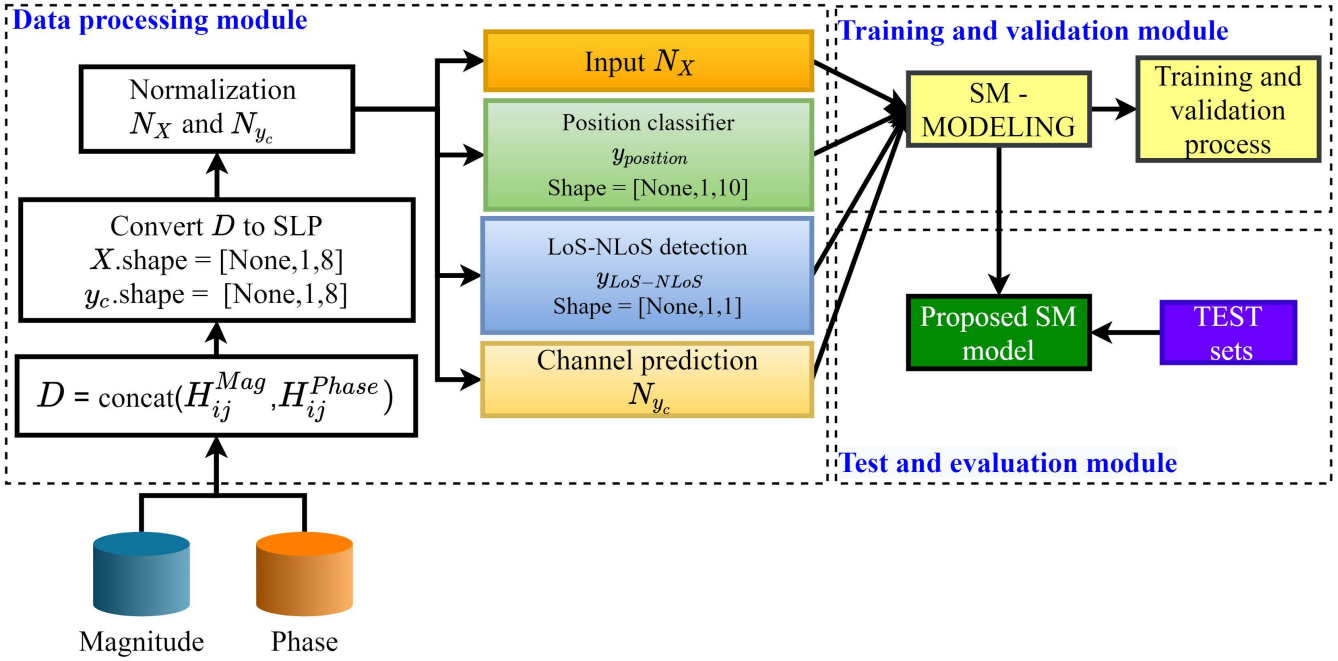

FIGURE 2. The modules used in the framework for SM modeling technique.

Then, training and validation modules were developed to ensure the efficiency of the model prediction by monitoring the learning curves (LCs) for channel prediction and classification. LCs allow the optimization of the internal parameters of the three DL stacked networks. Finally, the test and evaluation modules were established using test data when it (the module) had no prior information. The SM is validated experimentally with data collected in 2 × 2 2–2 MIMO system with a frequency band of 2.3 GHz - 2.5 GHz [4]. In MIMO systems, a $m_t \times n_t$ transfer channel matrix $\boldsymbol{H}$ is created, which represents the complex subchannel gains from the m_t transmitting to the n_t receiving antennas [5]. The channel matrix $\boldsymbol{H}$ for a 2 × 2 MIMO system is expressed as [1], [5]

$$\boldsymbol{H} = \begin{bmatrix} H_{11} & H_{12} \\ H_{21} & H_{22} \end{bmatrix}. \quad (1)$$

where H_{ij} represents the complex subchannel gain from the i^{th} transmitting antenna to the j^{th} receiving antenna.

A. MEASUREMENT PROCEDURE

The measurement procedure was carried out in a real gold mine (located in Val d'Or city in northern Quebec) within a gallery 90 m underground with a width and height of 4 m and 2.45 m, respectively (Figure 3 [4]). The underground mine environment is characterized by rough, random surfaces, and non-uniform gallery dimensions. The measurements were performed in a B2B configuration, as reported in [4]. Two antenna configurations were considered: co-positioned (CP) and 90 ° rotated antenna (90 deg) systems.

The measurement system setup consisted of a vector network analyzer (VNA), power amplifier, and low-noise amplifier connected to the transmitter (Tx) and receiver (Rx).

TABLE 1. Measurements scenario.

Polarization	Circular (Cir)			Linear
Scenario	CP-LoS	90 deg-LoS	CP-NLoS	CP-LoS
Positions	10	10	9	7

TABLE 2. Measurement system configuration.

Parameters	Values
Frequency	2.3GHz - 2.5 GHz
Transmitted power	-10 dBm
Average noise floor	-80 dBm
Bandwidth	200 MHz
Rx gain	6.6 dBi
Tx gain	6.6 dBi
Cable loss	0.6 dB/m
Antenna height (B2B)	1.50 m
Sweep time	60 s
Antenna types	Linearly and circularly polarized patch

The VNA was used to measure the magnitude and phase of the channel frequency response in the desired frequency range. During the measurements, the propagation channel was considered stationary for both scenarios. The Tx was placed at a fixed position (at the chest of a volunteer student), and the Rx (located at the chest of another volunteer student) was changed up to 10m away from the Tx, as shown in Figure 4. The positions of the different measurements and antenna configurations are listed in Table 1 for the LoS and

FIGURE 3. Measurement procedures within underground mine environment.

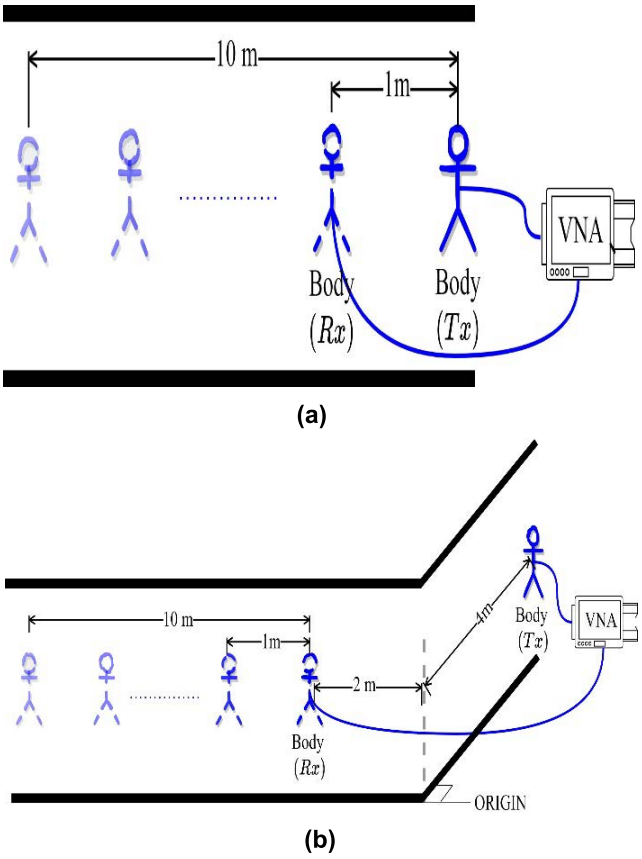

FIGURE 4. Experimental scenarios: (a) Los, (b) NLoS.

NLoS scenarios. The measurement parameters are listed in Table 2.

B. DATA PROCESSING

Data processing is illustrated in Figure.5. Following the experimental scenarios, the channel matrix magnitude and phase measurements were performed for up to 10 different positions. At each position, ten snapshots with 2049 samples were measured from 2.3 GHz to 2.5 GHz within sweep time of 60s. In fact, the nature of the time series data of the obtained measurements is useful for the design of the stacked model, as explained in [28]. Hence, these measurements are sequences that have been concatenated horizontally to provide a dataset for the training and validation processes.

$$D = \text{concat}\left(H_{ij}^{\text{Mag}}, H_{ij}^{\text{Phase}}\right). \tag{2}$$

where $i \in (1, 2)$; $j \in (1, 2)$ represent the transmitted and received links, respectively. The framework uses dataset D as a multivariate (multiple-variable) magnitude and phase dataset. Subsequently, to predict the four matrix subchannels at each position, the sequences were divided into input and output samples. To achieve a model with high accuracy in terms of classification and regression, the concept of a sliding window is adopted [30] to convert the problem into a supervised learning problem (SLP). Thus, this method resolves the problem of subchannel predictions. Specifically, regression and classification problems were simultaneously used in the stacked model. The input model is dataset X, while the output (y_c) is only used for channel prediction in the case of regression problems. As a result, three-dimensional (3-D) data shapes are created and organized according to the number of samples, features, and variables, as shown in Figure 5 as [None, 1,8]. It is worth mentioning that the statement in Figure 5 indicates that the number of raw materials can be changed during the training and validation processes. Different outputs are used for the classification problems. A binary output for LoS-NLoS $(y_{LoS-NLoS})$ detection was created, and a categorical output $(y_{position})$ with a matrix of ten features was created. However, all target outputs were 3-dimensional size. The input shape is shown in Figure 5, it can be noticed that eight parameters must be considered in the prediction along with two variables (magnitudes and phases) for each sub-channel matrix. In fact, it is complicated to use the three-stacked model to converge and achieve a high prediction accuracy in both regression and classification. As used in [28], the Z-core normalization [31] standard must be applied to shed the values between the magnitude and the phase without losing the relevant information of the model.

The Z-score normalization is described as follows [31]:

$$N_X = \frac{X - \mu_X}{\sigma_X}, \tag{3}$$

$$N_{y_c} = \frac{y_c - \mu_{y_c}}{\sigma_{y_c}}. \tag{4}$$

where μ, σ are the mean and standard deviations, respectively. Moreover, the input data are transformed into small batch size sequences [28] to facilitate the learning process and avoid gradient descent problems [32], [33].

III. TRAIN AND VALIDATION MECHANISM

The diagram in Figure 6 shows the high-level process of the proposed model. The stacked model was trained in the collected channel matrix H. Subsequently, the model was evaluated to test its capability to classify the position, LoS-NLoS identification, and channel prediction. Finally, using the prediction channel H, the channel characterization and modeling were compared with the model results of the published studies [4].

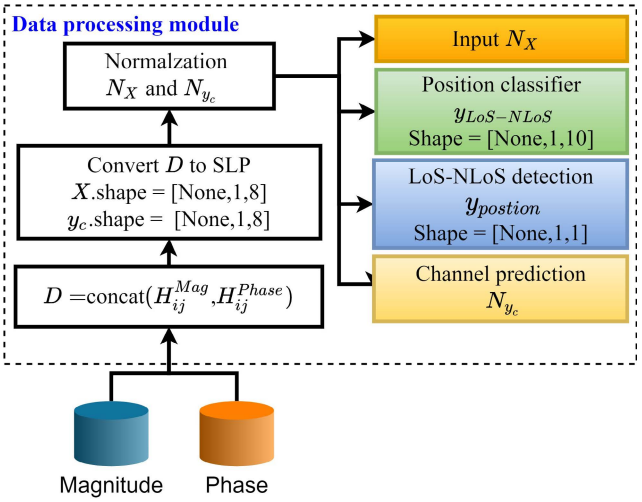

FIGURE 5. Data processing module.

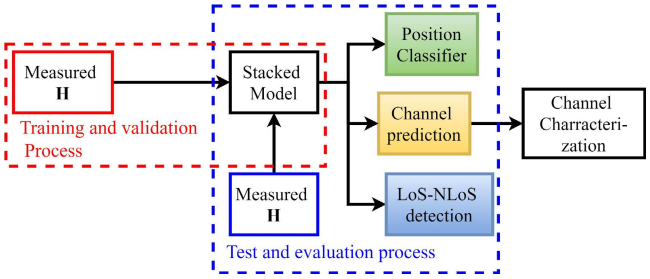

FIGURE 6. Proposed stack model diagram for channel prediction and classification.

After the data processing scheme, 1/3 and 2/3 of the normalized datasets were split into the validation and training datasets, respectively. The target datasets were different for classification and regression problems. The target outputs for the regression and classification are shown in Figure 8. For regression, the output N_{y_c} is used, where the impaired blue column (from 1 to 7) is the magnitude column and the pair yellow column (from 2 to 8) are the phase columns. On the other hand, for categorical classification, the position classification matrix output ($y_{position}$) is used, where up to ten positions are transformed to create a binary column for each category. Finally, the binary output ($y_{Los/NLoS}$) is used for LoS-NLoS detection, where the true green value (one) is for the LoS scenario and the false red value (zero) is for NLoS.

Prior to the SM model outputs, different losses were considered depending on the type of prediction problem, as shown in Figure 7.

For binary classification, binary cross-entropy loss (BCE) [34] is assigned, where it is compared to each of the predicted probabilities to the actual class output (LoS [one] or NLoS [zero]) [34], [35]. Before using BCE, a sigmoid function is applied independently to each element x_i of vector x in the last layer to squash the vector data range between 0 and 1. This is described as follows [36], [37]:

$$f\left(x_i\right) = \frac{1}{1 + e^{x_i}}. \tag{5}$$

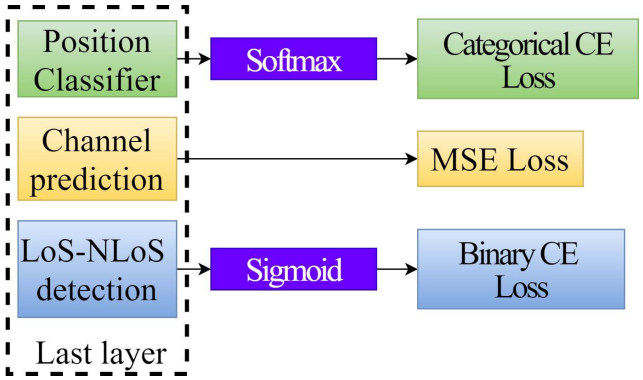

FIGURE 7. Activation functions and it losses metrics used in the SM.

Furthermore, distinct losses were evaluated in the multiclass classification of the position classifier. Categorical cross-entropy loss (CCE) [34] is chosen for this case, which has the same performance as BCE in the case of binary classification. However, a Softmax activation function is considered to calculate the probability of each target class's overall potential target classes. The probabilities obtained are useful in defining the target class for the inputs [38], [39]. The output probability range is the key benefit of adopting softmax. The probability range is from 0 to 1, and the total of all probabilities is one. When the Softmax function is used in a multi-classification model, the probability of each class is returned, with the target class having the highest one (probability) [54]–[57].

Therefore, the SM model uses SoftMax for position classification [36]–[39]:

$$f_s\left(x_i\right) = \frac{e^{x_i}}{\sum_j^k e^{x_j}}. \tag{6}$$

Once the input and target output data are settled, the training and validation processes are monitored by the learning curve (LC) [40]. Moreover, different problems with different approaches for quantifying LC are used. Figures 9, 10, and 11 show the BCE in terms of loss and accuracy for LoS-NLoS, and the MSE error in terms of percentage was used for channel prediction loss. Then, the CCE is calculated in terms of the loss and accuracy for position classification. Because the data are collected mostly in LoS scenarios (more than NLoS data), the SM model has difficulties learning in a proper manner. Specifically, the training process begins to be adjusted for the NLoS (more LoS data in the input). However, the data processing module assisted the model in adapting and predict appropriately the NLoS data, as shown in the Figure 8 high classification accuracy (up to 100%), as well as smaller BCE losses, were achieved by the stacked model for LoS-NLoS detection. A good agreement between the training and validation was obtained.

For the channel prediction in Figure 9, the MSE in terms of percentage was lower with respect to the training epochs. Moreover, the training loss decreased and started to settle in at approximately 300 epoch and 0.75% of MSE. Furthermore,

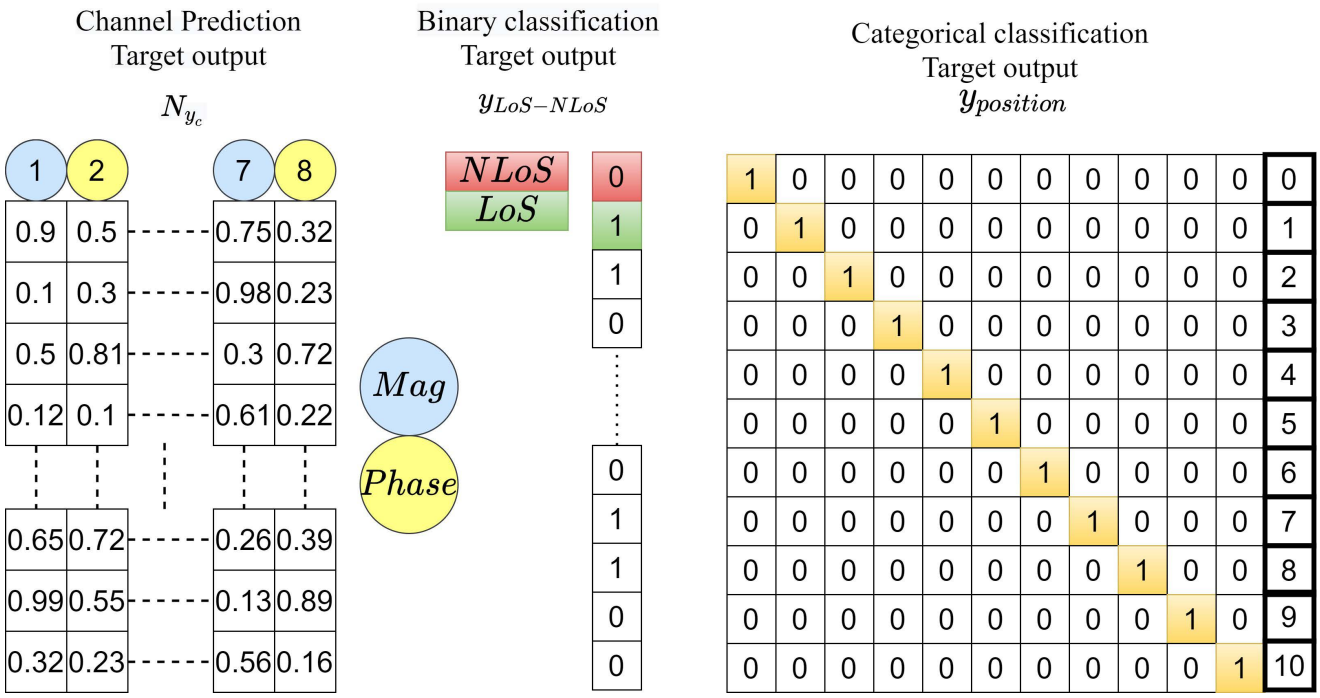

FIGURE 8. Target output for regression and classification.

high accuracy was observed up to 85% classification accuracy and lower CCE loss values in case of position classifiers (Figure 11).

Monitoring the learning curves is crucial for the model performance and accuracy of the test results. As described in [40], [41] a good fit must be fulfilled to ensure that the model learns sufficiently from the training sets, which is called underfitting, or the opposite of overfitting. However, as shown in these Figures 9, 10, and 11, the SM model learns appropriately to predict the test sets. Learning curves were obtained using the parameter model shown in Table 3. The dynamic learning rate schedule [42] was introduced to allow the learning model to incorporate some learning randomness once the learning rate is established at the lowest values [42].

The number of hidden layers and batch size were set as previously reported [28]. The dimensions of the input layer are the same as those of the input data (3D). The structure of the LSTM unit contains forget gate f_t, candidate layer $\bar{C}_t$, hidden state H_t, input gate I_t, output gate O_t and memory state C_t. The relevant mathematical formulas are as follows [28], [43]:

$$f_t = \sigma\left(X_t * \boldsymbol{W}_f + H_{t-1} * \boldsymbol{W}_f + b_f\right). \quad (7)$$

$$\bar{C}_t = Tanh\left(X_t * \boldsymbol{W}_{\bar{C}} + H_{t-1} * \boldsymbol{W}_{\bar{C}} + b_{\bar{C}}\right). \quad (8)$$

$$I_t = \sigma\left(X_t * \boldsymbol{W}_i + H_{t-1} * \boldsymbol{W}_i + b_i\right). \quad (9)$$

$$O_t = \sigma\left(X_t * \boldsymbol{W}_o + H_{t-1} * \boldsymbol{W}_o\right). \quad (10)$$

$$C_t = f_t * C_{t-1} + I_t * \bar{C}_t. \quad (11)$$

$$H_t = O_t * Tanh\left(C_t\right). \quad (12)$$

where X_t are the input vectors , H_{t-1} are the previous output cells , C_{t-1} are the previous memory cells , H_t are the current output cells , C_t are the current memory cells, $\boldsymbol{W}$,$\boldsymbol{b}$ are the weight matrices, and the bias vectors, respectively. Using a combination of these equations, the LSTM unit can be expressed as

$$\boldsymbol{h_t} = f\left(\boldsymbol{h}_{t-1}, \boldsymbol{x}_t, \boldsymbol{\psi}\right). \quad (13)$$

where f is the LSTM function, and ψ is the vector parameter(LSTM is employed in the SM encoder–decoder models [43]). Similarly, an adaptive moment estimation (Adam) optimizer is introduced to resolve the gradient descent problem. Adam is an optimization technique that can be used to update network weights iteratively based on training data, instead of the traditional stochastic gradient descent procedure [44]. The same results were observed after performing the same test as in [28] with the SM model, which justifies the use of identical simulation parameters.

IV. TEST AND EVALUATION MODULE

For the test and evaluation modules, data were extracted from the measured dataset. Therefore, data processing was performed along with training and validation data. Moreover, the module aims to test the model's capability to predict new samples, identify the position, and determine whether it belongs to LoS or NLoS scenarios. In this case, the model was evaluated at a distance of 5 m to predict the channel, classify the position, and LoS-NLoS detection.

A. CHANNEL MATRIX PREDICTION

For MIMO channel prediction, Figures 12 and 13 demonstrate each of the measured and predicted subchannels

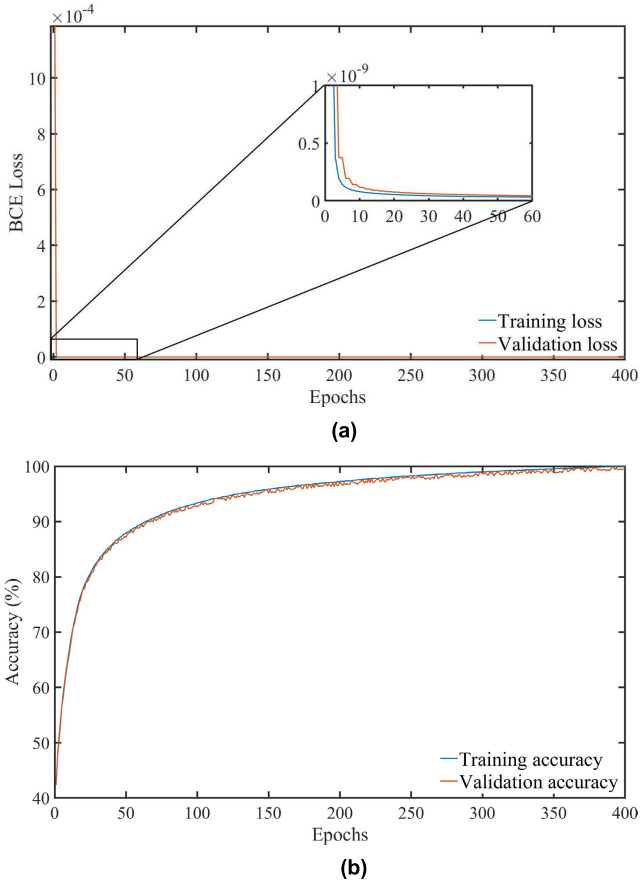

FIGURE 9. The training and validation learning curves for LoS-NLoS detection: (a) BCE loss curves, (b) accuracy classification curves.

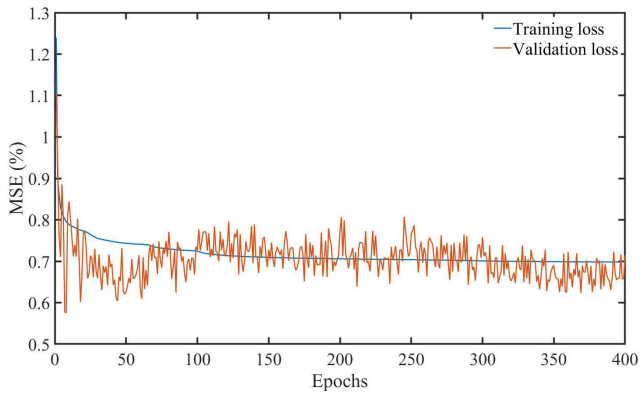

FIGURE 10. MSE loss in term of percentage for channel matrix prediction.

of matrix $\boldsymbol{H}$ within different antenna configurations. The variables Mag($\boldsymbol{H}$) and phase ($\boldsymbol{H}$) are shown at 5 m. Nevertheless, the root-mean-square error (RMSE) in terms of percentage was used to quantify the prediction losses [45] as illustrated in Figure 14. It is observed that the RMSE errors are low for all sub-channels' magnitudes (between 0.6% and 2.6%) and phase prediction (between 4% and 16%). Owing to the data difference between Mag($\boldsymbol{H}$) and Phase($\boldsymbol{H}$), the RMSE values for the magnitude are less than the phase RMSE values. The model first learns Mag($\boldsymbol{H}$) and

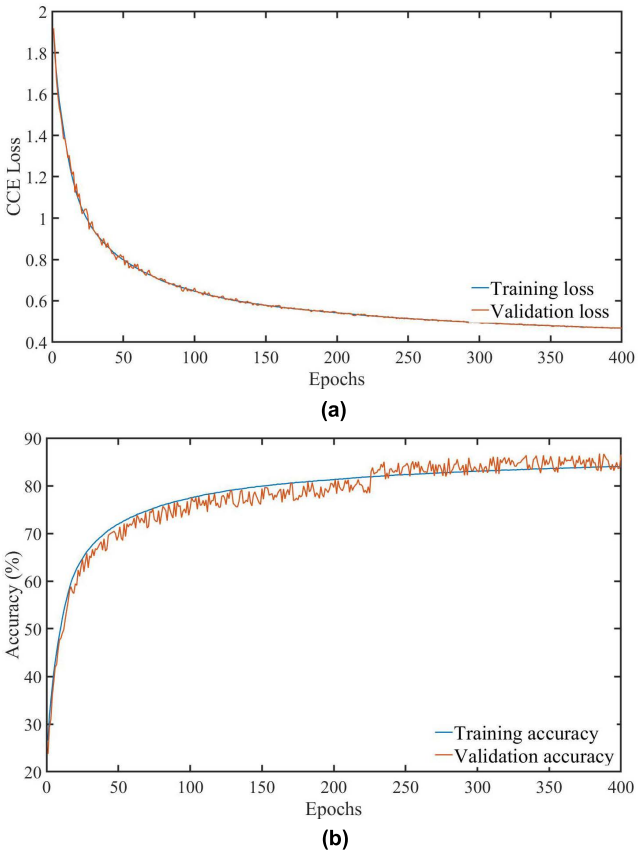

FIGURE 11. The training and the validation learning curves for position classification: (a) CCE Loss curves, (b) accuracy classification curves.

TABLE 3. Simulation parameters.

Parameters	Stacked model		
	Position classifier	Channel prediction	LoS-NLoS detection
Hidden layers	100		
Batch size	100		
Loss functions	CCE	MSE	BCE
Training dataset size	136 600		
Validation dataset size	68300		
Optimizer	Adam		
Learning rate	0.001		

Phase($\boldsymbol{H}$), as shown in Figure 8, where Mag($\boldsymbol{H}$) occurs earlier than Phase ($\boldsymbol{H}$). Consequently, the model is more capable of performing in magnitude than phase data. It can be seen that for the circular polarization (90 deg-CIR and CP-CIR) LOS scenario, the RMSE values are better than those for the linear polarization (CP-LIN) scenarios, as well as the CIR RMSE values in the NLoS scenarios. This is due to the fact that the datasets are not well balanced in the scenarios with lesser RMSE due to the availability of S-parameter measurements in CIR and LoS topologies. However, this does not affect model learning, which is well illustrated by the learning curves.

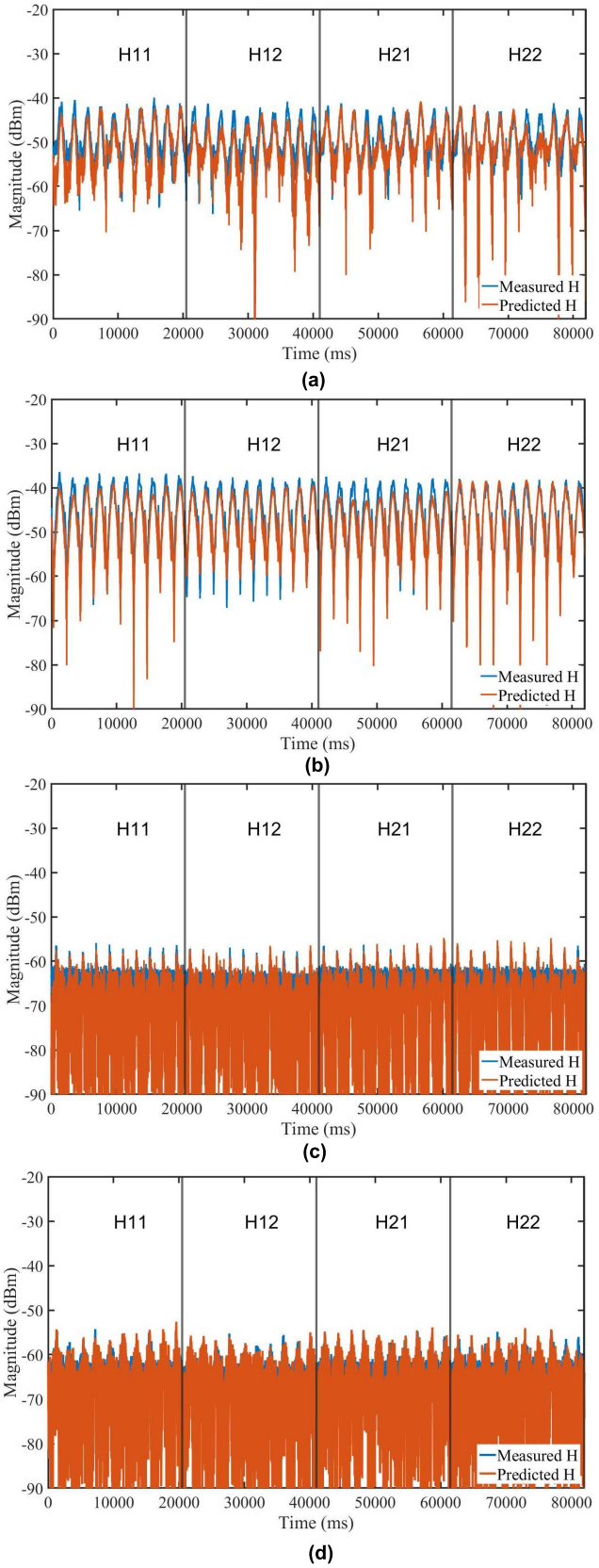

FIGURE 12. Measured and predicted channel matrix magnitude (Mag(H)) at 5m for different antenna configurations: (a) 90deg-CIR, (b) CP-CIR, (c) CP-LIN, and (d) CP-LIN-NLOS.

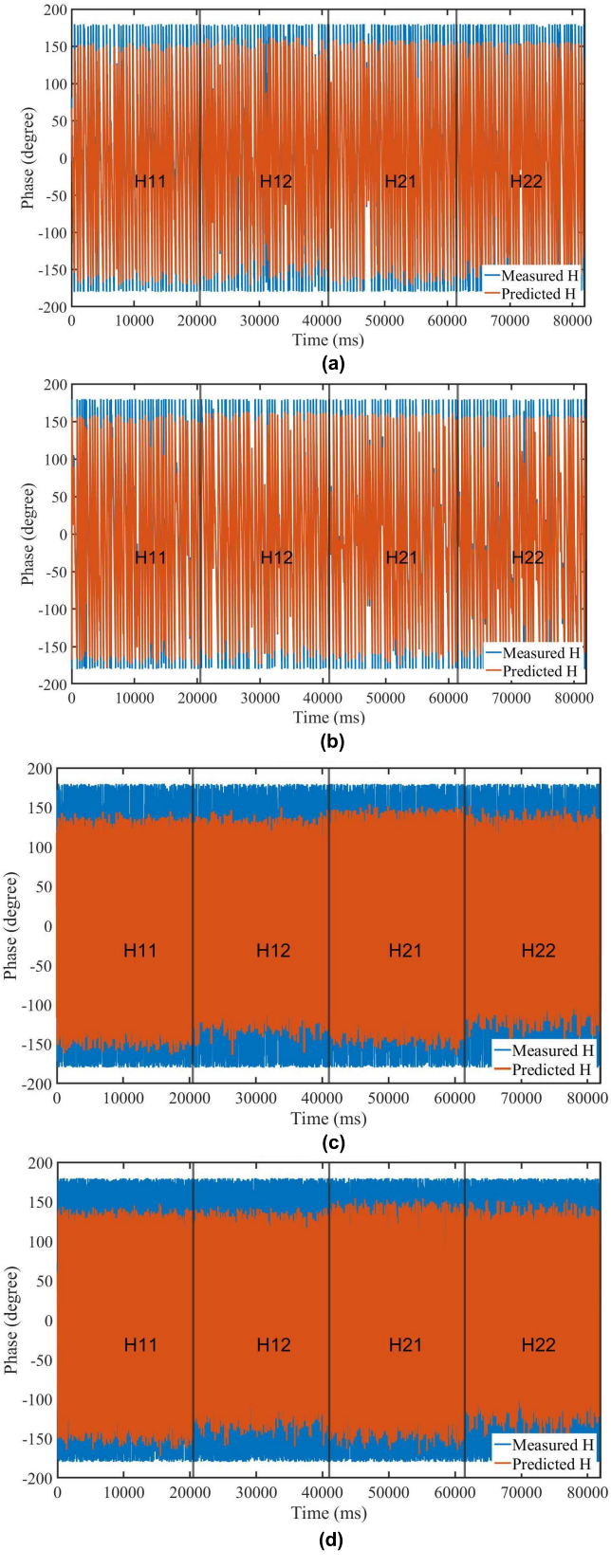

FIGURE 13. Measured and predicted channel matrix phase (Phase(*H*)) at 5m for different antenna configurations: (a) 90deg-CIR, (b) CP-CIR, (c) CP-LIN, and (d) CP-LIN-NLOS.

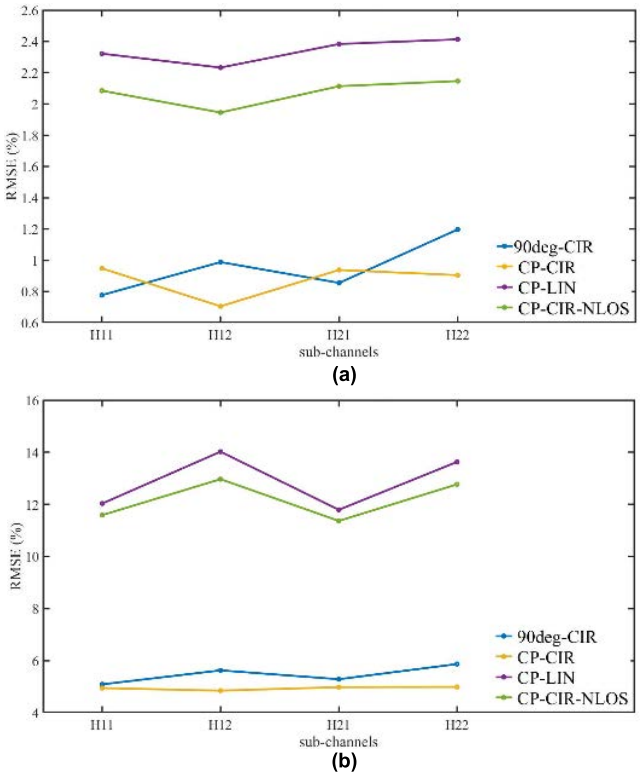

FIGURE 14. RMSE evaluation for channel prediction: (a) Magnitude and (b) Phase.

B. LoS-NLoS IDENTIFIER AND POSITION CLASSIFIER

This section presents the classification results. Moreover, as demonstrated by the training and validation processes, the model achieved an efficient prediction process in terms of loss and accuracy. In the one hand, The confusion matrix (CM) [46] is used in the case of classification. The CM is considered as a summary of the prediction results for any classification problem in the machine learning field. It quantifies the number of correct and incorrect predictions of the model. Therefore, when the classification model generates predictions, the CM displays how it gets confused [40].

The CM results are shown in Figures 15 and 16. The position classification (Figure 15) is shown by considering a multiple-class classification (up to 10 positions). The SM achieved up to 87% accuracy prediction in terms of classification within all the antenna configurations. Even though the SM is trained to classify 10 positions (output feature shape is 10), it is capable of predicting the data from different positions in different configurations with missing information, as illustrated in Table 1. Hence, the proposed model shows its capability to predict positions within all configurations with fewer collected positions, such as the CP-LIN-LOS and CP-CIR-NLoS configurations, where only seven and nine positions were measured, respectively.

Regarding the LoS-NLoS detection, the model achieved up to 100 % classification accuracy, as demonstrated by the LC. Therefore, CM is also used (Figure 16) in this case, which is considered as a binary output, where 0 and 1 refer

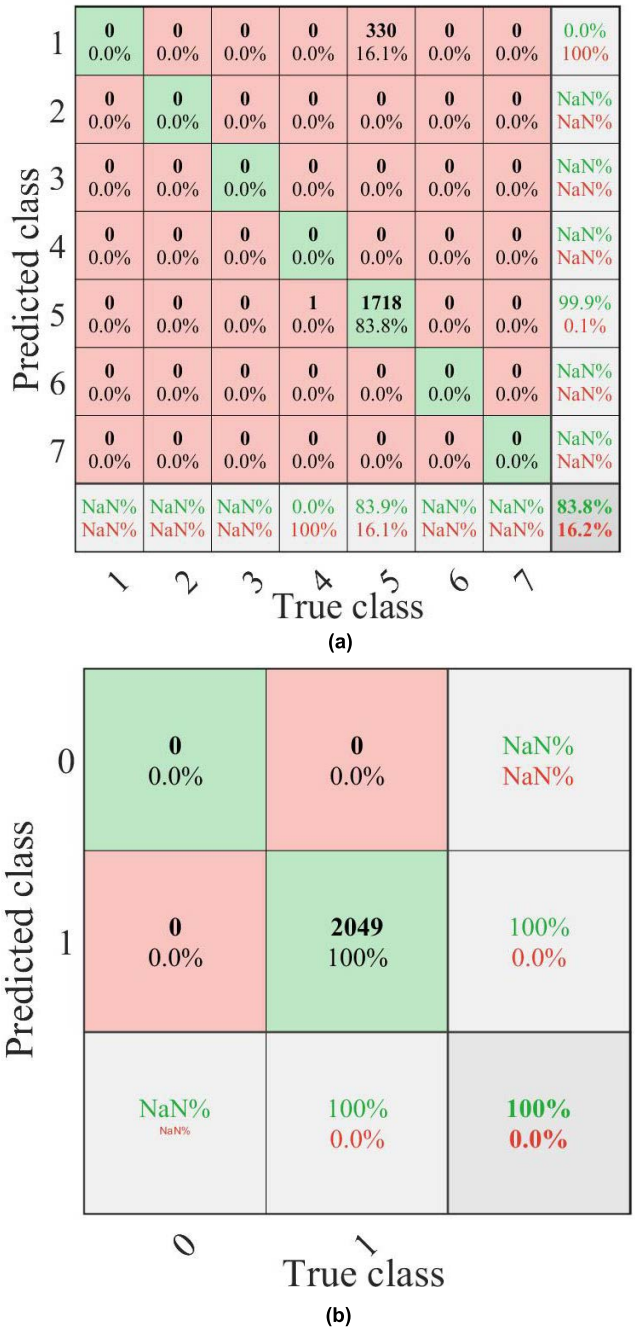

FIGURE 15. Confusion matrix for CP-LIN configuration in LoS scenario: (a) position classifier, (b) LoS-NLoS detection (LoS: 1 and NLoS: 0).

to NLoS and LoS, respectively. It is worth mentioning that more data samples were collected in LoS scenario than NLOS one. However, the LC shows that the SM learns properly to classify all samples within both LoS and NLoS scenarios. In both classifications, SM aims to classify every sample collected at every position. Therefore, the SM classifies a sample collected at a position of 5m in the LoS and NLoS scenarios. The classification of the collected samples in the position 5 was evaluated with 83.8% of accuracy using the CP-LIN configuration in LoS scenario. As illustrated in Figure 15(a),

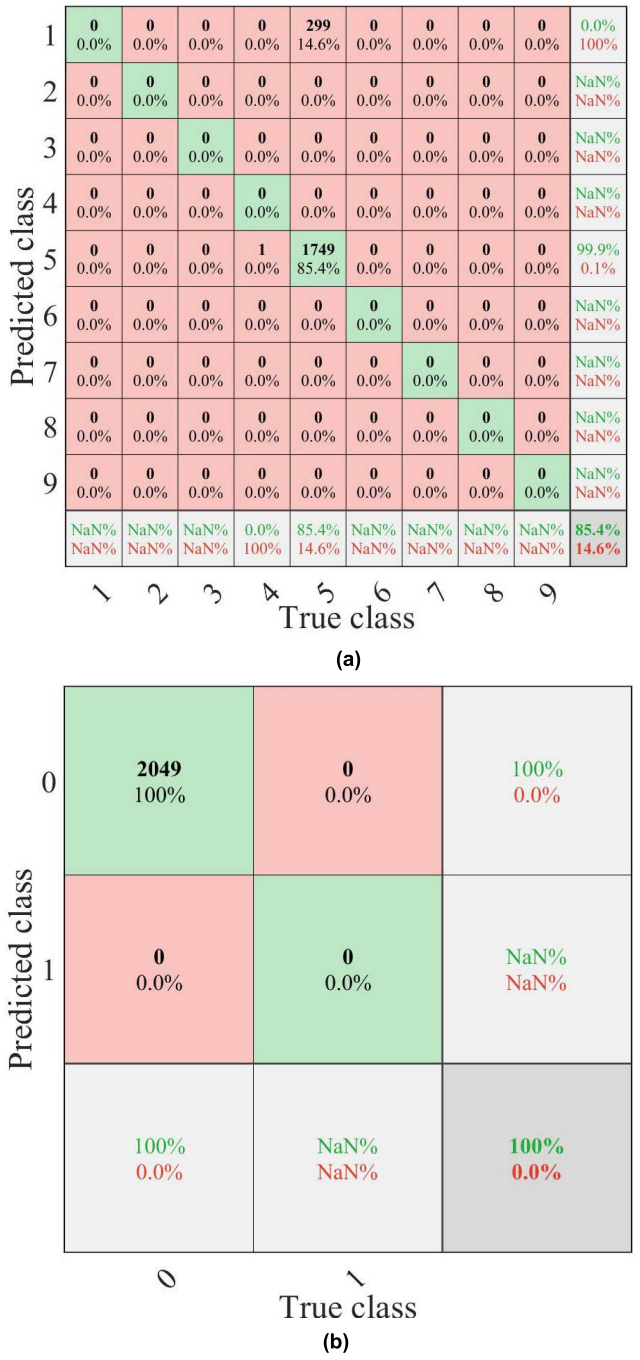

FIGURE 16. Confusion matrix for CP-CIR configuration in NLoS scenario: (a) position classifier, (b) LoS-NLoS detection (LoS: 1 and NLoS: 0).

1718 samples were correctly classified as of, whereas the rest of the samples were classified incorrectly between positions 1 and 10. Similarly, as for CP—CIR configuration in NLoS scenario, 85.4% of accuracy was achieved by the SM, where 1749 samples were correctly classified. Hence, a slightly more significant incorrect sample classification (14.6%) was observed, as illustrated in Figure 15. This implies that even though the model is learning well, it is challenging for the SM model to predict all the positions of the NLoS samples. This is because of the collected measurements, where additional

TABLE 4. Measurements scenario.

Polarization		Circular			Linear
Scenarios		CP-LOS	90 deg-LOS	CP-NLOS	CP-LOS
PL exponent	Published [4]	2.33	1.71	2.18	1.26
	Predicted	2.38	1.77	2.56	1.70

balanced datasets are needed to reach up to approximately the 100% of prediction accuracy. In fact, the collected position samples were not sufficiently balanced, which did not optimize the SM prediction in a multiple-class classification. In contrast, LoS-NLoS detection was well predicted in both configurations. Therefore, a 100% accuracy was achieved by the SM. Hence, the collected measured datasets were sufficient for the SM to identify the difference between the binary results (zero for NLoS and one for LoS).

V. CHANNEL CHARACTERIZATION AND MODELING

In this section, the magnitude and phase were used to evaluate the path loss and channel modeling for comparison with the measured values published by Elazhari [4].

A. PATH LOSS

L is defined as signal attenuation caused by environmental effects. This was obtained by applying the following equation [4]

$$PL\,(d) = PL\,(d_0) + 10.\beta.\log_{10}\left(\frac{d}{d_0}\right) + \mathrm{X}. \qquad (14)$$

where $PL\,(d_0)$ represents the mean path loss at reference d_0, d is the Tx-Rx distance where the path loss is calculated. β is the path loss exponent estimated by using the linear regression analysis, and X(dB) is the zero mean Gaussian variable. As observed from the linear analysis, the values of the path loss exponent of the antenna configurations were evaluated and are illustrated in Table 4. Figure 17 shows the predicted and measured PL, PPL, and MPL, respectively. The predicted calculated PL exhibited the same behavior as the measured calculated ones. These results illustrate the efficiency of the SM prediction results, where the same observations can be used as the measured ones.

B. CHANNEL MODELING

As mentioned in [4], channel modeling involves developing an impulse response to describe a single-input single-output body-to-body (SISO - B2B) system in a mining environment that is characterized by rough and random surfaces. The impulse response was presented in [4].

$$h\,(t) = \sum_{i=0}^{N-1} a_i \delta\,(t - t_i)\, e^{j\theta_i}. \qquad (15)$$

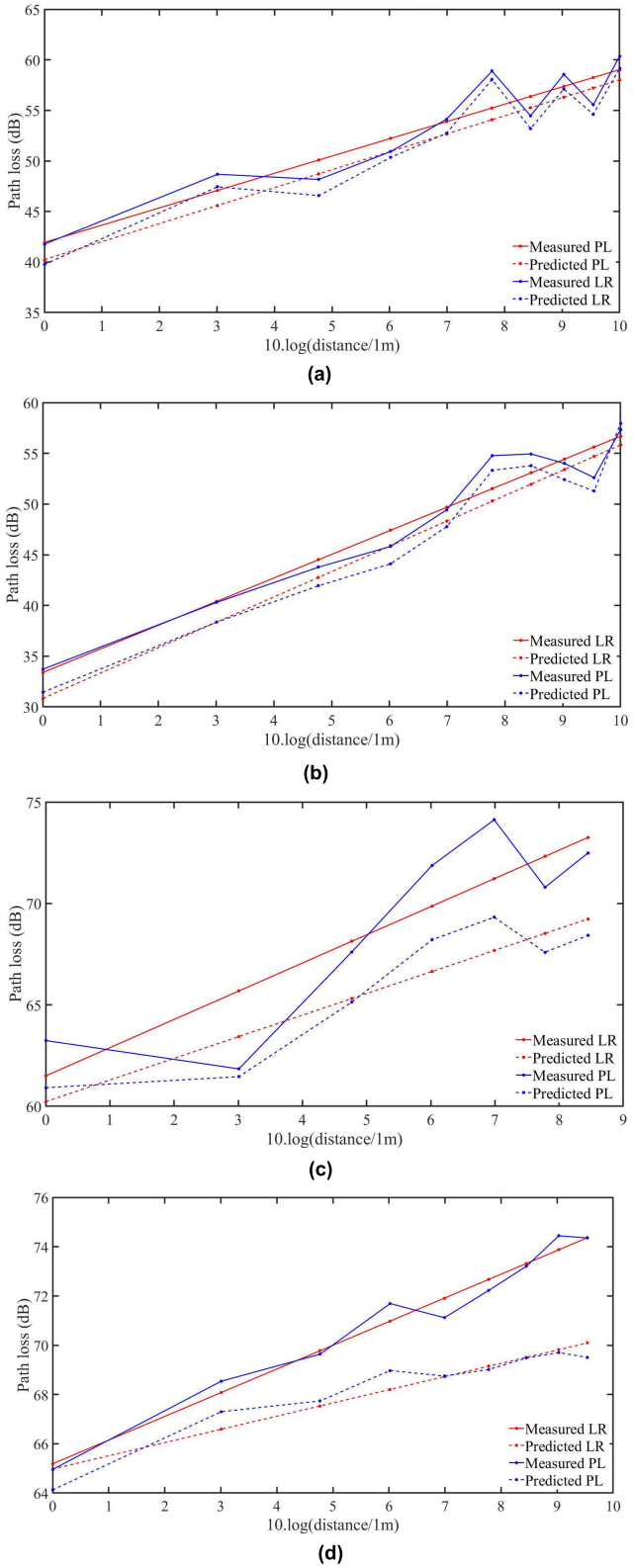

FIGURE 17. MPL, PPL and linear regression (LR) model results: (a) 90deg-CIR, (b) CP-CIR, (c) CP-LIN, and (d) CP-LIN-NLOS.

where N is the number of multipath components, a_i, t_i and θ_i are the random amplitude, arrival time, and phase of the i^{th} multipath component, respectively. δ denotes the Kronecker delta function. Regarding the modeling procedures reported in [4], two modeling procedures are discussed in terms of path amplitudes and arrival times. The path amplitude a_i is modeled as an independent complex Gaussian random variable with an average power that follows the exponential power delay profile. The time arrivals of the multipath components were derived from measurements [4]. In this section, the SM impulse response model is compared with the measured and stochastic empirical (SE) modeled impulse response, as illustrated in Figure 18. Table 5 lists the MSE values obtained by the SM and stochastic models. It can be observed that the SM model MSE is the lowest, which provides more accuracy than the stochastic model to describe the impulse response for the body-to-body channel.

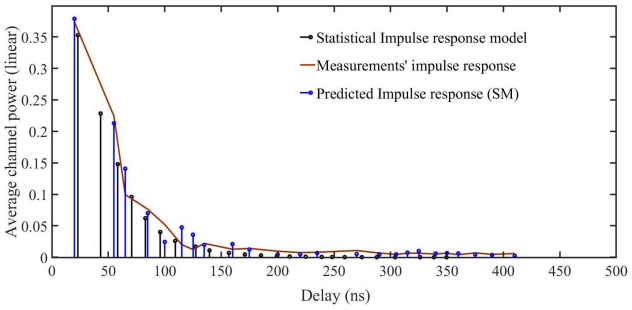

FIGURE 18. SM impulse response model compared to both stochastic empirical (SE) and measurement impulse response.

TABLE 5. IR model performance.

	SE model	SM model
MSE	1.8437e-04.	1.7250e-04

VI. CONCLUSION

In this paper, a new efficient MIMO channel model based on a deep learning algorithm is presented. A stacked model is introduced to predict the channel magnitude and phase for each subchannel of the channel matrix H. Then, it classifies the position where the measurements were collected for the LoS and NLoS scenarios. Moreover, different output losses were applied to measure both the classification and channel prediction problems. Published results were used to validate the SM model. The SM has achieved high accuracy in terms of performance assessment of the classification up to 100% for LoS and NLoS detection and channel prediction with lower RMSE. Using a multiple position classifier, the model showed its capability to predict the position, as shown at position 5m. However, the model struggles to predict the NLoS position owing to data imbalance. From the perspective of performance, the model is efficient because the prediction results are used for channel characterization and modelling. The model was validated by estimating each subchannel, position classifier, and LoS-NLoS detection while considering antenna diversity in underground mine environments.

The promising results revealed in this paper could lead to more research in deep learning and other aspects such as cloud technology use of wireless communications systems in indoor and outdoor environments.

REFERENCES

[1] I. B. Mabrouk, L. Talbi, and M. Nedil, "Performance evaluation of a MIMO system in underground mine gallery," *IEEE Antennas Wireless Propag. Lett.*, vol. 11, pp. 830–833, 2012.
[2] C. Formisano, D. Pavia, L. Gurgen, T. Yonezawa, J. A. Galache, K. Doguchi, and I. Matranga, "The advantages of IoT and cloud applied to smart cities," in *Proc. 3rd Int. Conf. Future Internet Things Cloud*, Aug. 2015, pp. 325–332.
[3] S. K. Routray, A. Javali, A. Sahoo, K. P. Sharmila, and S. Anand, "Military applications of satellite based IoT," in *Proc. 3rd Int. Conf. Smart Syst. Inventive Technol. (ICSSIT)*, Aug. 2020, pp. 122–127.
[4] M. E. H. El-Azhari, L. Talbi, and M. Nedil, "Body-to-body channel characterization and modeling inside an underground mine," *IEEE Trans. Antennas Propag.*, vol. 68, no. 6, pp. 4799–4809, Jun. 2020.
[5] I. B. Mabrouk, L. Talbi, M. Nedil, and K. Hettak, "MIMO-UWB channel characterization within an underground mine gallery," *IEEE Trans. Antennas Propag.*, vol. 60, no. 10, pp. 4866–4874, Oct. 2012.
[6] I. B. Mabrouk, L. Talbi, M. Nedil, Y. Coulibaly, and T. A. Denidni, "Effect of antenna directivity on performance of multiple input multiple output systems in an underground gold mine," *IET Microw., Antennas Propag.*, vol. 6, no. 5, pp. 555–561, Apr. 2012.
[7] M. E. Azhari, M. Nedil, I. B. Mabrouk, and L. Talbi, "Multipath effect on off-body channel parametters of a MIMO system using patch antennas inside a mine," in *Proc. IEEE Int. Symp. Antennas Propag. (APSURSI)*, Jun. 2016, pp. 1693–1694.
[8] M. E. Azhari, M. Nedil, I. B. Mabrouk, and L. Talbi, "Path loss effect on off-body channel capacity of a MIMO system using patch antennas inside a mine," in *Proc. IEEE Int. Symp. Antennas Propag. (APSURSI)*, Jun. 2016, pp. 1697–1698.
[9] H. M. El-Azhari, M. Nedil, I. B. Mabrouk, and L. Talbi, "Off-body channel characterization at 2.45 GHz in underground mine environment," in *Proc. IEEE Antennas Propag. Soc. Int. Symp. (APSURSI)*, Jul. 2014, pp. 251–252.
[10] L. Arabi, "Caractérisation du canal minier souterrain en utilisant des antennes à polarisation circulaire," Ph.D. dissertation, Dept. École d'ingénieurs, Université du Québec en Abitibi-Témiscamingue, Rouyn-Noranda, QC, Canada, 2018.
[11] A. A. M. Saleh and R. A. Valenzuela, "A statistical model for indoor multipath propagation," *IEEE J. Sel. Areas Commun.*, vol. JSAC-5, no. 2, pp. 128–137, Feb. 1987.
[12] S. Piersanti, L. A. Annoni, and D. Cassioli, "Millimeter waves channel measurements and path loss models," in *Proc. IEEE Int. Conf. Commun. (ICC)*, Jun. 2012, pp. 4552–4556.
[13] T. S. Rappaport, "Mobile radio propagation: Small scale fading and multipath," in *Wireless Communications Principles and Practice*, 2nd ed. Hoboken, NJ, USA: Prentice-Hall, 2001.
[14] T. S. Rappaport, *Wireless Communications: Principles and Practice*. Hoboken, NJ, USA: Prentice-Hall, 1996.
[15] I. Goodfellow, Y. Bengio, A. Courville, and Y. Bengio, *Deep Learning*. Cambridge, MA, USA: MIT Press, 2016.
[16] W. Andrew, C. Greatwood, and T. Burghardt, "Visual localisation and individual identification of Holstein friesian cattle via deep learning," in *Proc. IEEE Int. Conf. Comput. Vis. Workshops (ICCVW)*, Oct. 2017, pp. 2850–2859.
[17] W. Jiang and H. D. Schotten, "Deep learning for fading channel prediction," *IEEE Open J. Commun. Soc.*, vol. 1, pp. 320–332, 2020.
[18] T. Ding and A. Hirose, "Fading channel prediction based on complex-valued neural networks in frequency domain," in *Proc. Int. Symp. Electromagn. Theory*, 2013, pp. 640–643.
[19] W. Jiang and H. D. Schotten, "Recurrent neural network-based frequency-domain channel prediction for wideband communications," in *Proc. IEEE 89th Veh. Technol. Conf. (VTC)*, Apr. 2019, pp. 1–6.
[20] J. Fan, S. Chen, X. Luo, Y. Zhang, and G. Y. Li, "A machine learning approach for hierarchical localization based on multipath MIMO fingerprints," *IEEE Commun. Lett.*, vol. 23, no. 10, pp. 1765–1768, Oct. 2019.
[21] J. Yuan, H. Q. Ngo, and M. Matthaiou, "Machine learning-based channel estimation in massive MIMO with channel aging," in *Proc. IEEE 20th Int. Workshop Signal Process. Adv. Wireless Commun. (SPAWC)*, Jul. 2019, pp. 1–5.
[22] T. J. O'Shea, T. Erpek, and T. C. Clancy, "Deep learning based MIMO communications," 2017, *arXiv:1707.07980*.
[23] M. Arnold, S. Dorner, S. Cammerer, and S. T. Brink, "On deep learning-based massive MIMO indoor user localization," in *Proc. IEEE 19th Int. Workshop Signal Process. Adv. Wireless Commun. (SPAWC)*, Jun. 2018, pp. 1–5.
[24] S. Kim, S. Hong, M. Joh, and S.-K. Song, "DeepRain: ConvLSTM network for precipitation prediction using multichannel radar data," 2017, *arXiv:1711.02316*.
[25] Q. An, Z. Tao, X. Xu, M. El-Mansori, and M. Chen, "A data-driven model for milling tool remaining useful life prediction with convolutional and stacked LSTM network," *Measurement*, vol. 154, Mar. 2020, Art. no. 107461.
[26] L. Sun, Y. Wang, J. He, H. Li, D. Peng, and Y. Wang, "A stacked LSTM for atrial fibrillation prediction based on multivariate ECGs," *Health Inf. Sci. Syst.*, vol. 8, no. 1, pp. 1–7, Dec. 2020.
[27] K. A. Althelaya, E.-S.-M. El-Alfy, and S. Mohammed, "Stock market forecast using multivariate analysis with bidirectional and stacked (LSTM, GRU)," in *Proc. 21st Saudi Comput. Soc. Nat. Comput. Conf. (NCC)*, Apr. 2018, pp. 1–7.
[28] K. Kedjar, L. Talbi, and M. Nedil, "Efficient indoor propagation channel prediction based on deep learning approach," *IET Microw., Antennas Propag.*, vol. 15, no. 13, pp. 1671–1687, Oct. 2021.
[29] G. Arulampalam and A. Bouzerdoum, "A generalized feedforward neural network architecture for classification and regression," *Neural Netw.*, vol. 16, nos. 5–6, pp. 561–568, 2003.
[30] S. S. Joshi, "Calibrating recurrent sliding window classifiers for sequential supervised learning," M.S. thesis, Dept. Comput. Sci., Oregon State Univ., Corvallis, OR, USA, 2003.
[31] S. G. K. Patro and K. K. Sahu, "Normalization: A preprocessing stage," 2015, *arXiv:1503.06462*.
[32] R. Ge, F. Huang, C. Jin, and Y. Yuan, "Escaping from saddle points-online stochastic gradient for tensor decomposition," in *Proc. Conf. Learn. Theory*, 2015, pp. 797–842.
[33] S. Hochreiter, "The vanishing gradient problem during learning recurrent neural nets and problem solutions," *Uncertain. Fuzziness Knowl.-Based Syst.*, vol. 6, no. 2, pp. 107–116, Jun. 1998.
[34] Z. Zhang and M. R. Sabuncu, "Generalized cross entropy loss for training deep neural networks with noisy labels," 2018, *arXiv:1805.07836*.
[35] A. Buja, W. Stuetzle, and Y. Shen, "Loss functions for binary class probability estimation and classification: Structure and applications," *Work. Draft*, vol. 3, p. 13, Nov. 2005.
[36] C. Nwankpa, W. Ijomah, A. Gachagan, and S. Marshall, "Activation functions: Comparison of trends in practice and research for deep learning," 2018, *arXiv:1811.03378*.
[37] T. Szandała, "Review and comparison of commonly used activation functions for deep neural networks," in *Bio-Inspired Neurocomputing* (Studies in Computational Intelligence). Berlin, Germany: Springer, 2021, pp. 203–224.
[38] M. Wang, S. Lu, D. Zhu, J. Lin, and Z. Wang, "A high-speed and low-complexity architecture for softmax function in deep learning," in *Proc. IEEE Asia Pacific Conf. Circuits Syst. (APCCAS)*, Oct. 2018, pp. 223–226.
[39] A. F. Agarap, "Deep learning using rectified linear units (ReLU)," 2018, *arXiv:1803.08375*.
[40] J. Brownlee, *Better Deep Learning: Train Faster, Reduce Overfitting, and Make Better Predictions*. Machine Learning Mastery, 2018. [Online]. Available: https://machinelearningmastery.com/
[41] M. J. Anzanello and F. S. Fogliatto, "Learning curve models and applications: Literature review and research directions," *Int. J. Ind. Ergonom.*, vol. 41, no. 5, pp. 573–583, Sep. 2011.
[42] M. D. Zeiler, "ADADELTA: An adaptive learning rate method," 2012, *arXiv:1212.5701*.
[43] P. Malhotra, A. Ramakrishnan, G. Anand, L. Vig, P. Agarwal, and G. Shroff, "LSTM-based encoder–decoder for multi-sensor anomaly detection," 2016, *arXiv:1607.00148*.
[44] D. P. Kingma and J. Ba, "Adam: A method for stochastic optimization," 2014, *arXiv:1412.6980*.

[45] A. Botchkarev, "Performance metrics (error measures) in machine learning regression, forecasting and prognostics: Properties and typology," 2018, *arXiv:1809.03006*.
[46] P. Trajdos and M. Kurzynski, "A dynamic model of classifier competence based on the local fuzzy confusion matrix and the random reference classifier," *Int. J. Appl. Math. Comput. Sci.*, vol. 26, no. 1, pp. 175–189, Mar. 2016.

KHALED KEDJAR (Member, IEEE) received the bachelor's and master's degrees in electrical and electronics engineering from the University of Boumerdès, Algeria. He is currently pursuing the Ph.D. degree with the University of Quebec in Outaouais (UQO). He is a Researcher with the Telebec Underground Communications Research Laboratory (LRTCS). He is currently working as a part-time Lecturer with UQO, a reviewer of IEEE Access, and a Cloud IoT Analyst of CGI Inc. His research interests include radio wave propagation, multiple-input and multiple-output systems, and the application of deep learning algorithms in RF propagation modeling and measurement campaigns in indoor complex environments.

MOULAY ELHASSAN ELAZHARI (Member, IEEE) received the bachelor's and master's degrees in electrical and electronics engineering from California State University, Sacramento (CSUS), in 2005 and 2008, respectively, the master's degree in telecommunications engineering from the University of Quebec, Abitibi-Témiscamingue, in 2015, and the Ph.D. degree from the University of Quebec in Outaouai (UQO), in 2020. He worked as an Electrical Engineer with the Motion Control Engineering Research and Development Department, from 2007 to 2011; and has been with the Research and Development Department of Meglab Inc., since 2016. He also served as a Researcher for the Telebec Underground Communications Research Laboratory (LRTCS), from 20013 to 2020; and is currently working as an Assistant Professor with School of Science and Engineering, Al Akhawayn University, Morocco. His research interests include radio-wave propagation for multiple-input and multiple-output systems, body area networks, and robotic manipulators.

LARBI TALBI (Senior Member, IEEE) received the M.S. and Ph.D. degrees in electrical engineering from Laval University, Quebec, QC, Canada, in 1989 and 1994, respectively. He completed a postdoctoral fellowship with INRS-Telecommunications, Montreal, QC, within the Personal Communications Research Group, from 1994 to 1995, where he led projects supported by Bell Canada. From 1995 to 1998, he was an Assistant Professor with the Electronics Engineering Department, Riyadh College of Technology, Saudi Arabia. During 1998 to 1999, he was an Invited Professor with the Electrical and Computer Engineering Department, Laval University. Since 1999, he has been a Professor with the Department of Computer Science and Engineering, University of Quebec, Outaouais/Ottawa region, Canada, where he is M.Sc. Program Chair in sciences and information technologies. He has authored or coauthored more than 170 journal articles and conference papers. His research interests include the experimental characterization and modeling of UHF/EHF indoor radio propagation channels and the design of antennas and microwave circuits for wireless communication systems. Currently, he is actively involved in major projects related to the deployment of wireless technologies in underground mines, mainly experimental characterization of underground mine channels using MIMO antennas at 60 GHz, the design of microwave and RF components using SIW techniques and metamaterials, and antenna arrays for wireless applications. He is a member of Ordre des Ingénieurs du Québec.

MOURAD NEDIL (Senior Member, IEEE) received the Dipl.Ing. degree from the University of Algiers (USTHB), Algeria, in 1996, the D.E.A. (M.S.) degree from the University of Marne la Vallée, Marne-la-Vallée, France, in 2000, and the Ph.D. degree from the Institut National de la Recherche Scientifique (INRS-EMT), Université de Québec, Montreal, QC, Canada, in April 2006. He completed a postdoctoral fellowship at the INRS-EMT within the RF Communications Systems Group, from 2006 to 2008. In June 2008, he joined the Engineering School Department, University of Quebec at Abitibi-Témiscamingue, Quebec, Canada, where he is currently a Full Professor. His research interests include antennas, MIMO radio wave propagation, and microwave devices.